



## Investigation of precipitation kinetics of FeCO<sub>3</sub> by EQCM

Zheng Ma\*, Yang Yang, Bruce Brown, Srdjan Nescic, Marc Singer

Institute for Corrosion and Multiphase Technology, Department of Chemical & Biomolecular Engineering, Ohio University 342 West State Street, Athens, OH 45701 USA



### ARTICLE INFO

#### Keywords:

EQCM

Carbon dioxide corrosion

Iron carbonate precipitation kinetics

### ABSTRACT

Iron carbonate (FeCO<sub>3</sub>) is the most common corrosion product in aqueous CO<sub>2</sub> corrosion of mild steel. When it forms, the FeCO<sub>3</sub> corrosion product layer may be protective, by serving as a diffusion barrier and by affecting the rate of electrochemical reactions at the surface. In the present study, an Electrochemical Quartz Crystal Microbalance (EQCM) was used to investigate the kinetics of precipitation of FeCO<sub>3</sub> from an aqueous CO<sub>2</sub> corrosion environment. EQCM is a technique providing very accurate *in-situ* measurement of surface mass change, enabling also simultaneous electrochemical measurements. Three different substrates were used to conduct the FeCO<sub>3</sub> precipitation experiments: a cathodically polarized gold-coated quartz crystal, a freely corroding iron-coated quartz crystal and a cathodically polarized iron-coated quartz crystal, at varied temperatures (50–80 °C). Precipitation rates of FeCO<sub>3</sub> obtained by using EQCM were repeatable and consistent across different substrates. The obtained precipitation rates were used to determine the theoretical kinetic constant and the activation energy, which was then compared with those reported in the Sun and Nescic model (2008). Discrepancies between the predicted and experimental values were noticed at lower saturation levels and improvements in the model are proposed.

### 1. Introduction

In the oil and gas industry, corrosion prevention and control is a critical and challenging issue as the internal corrosion of pipeline is encountered during daily operation. Being one of the most common corrosion types, the aqueous CO<sub>2</sub> corrosion of carbon steel and the formation of FeCO<sub>3</sub> comprise of a complex system of interrelated processes that include homogenous aqueous CO<sub>2</sub> chemical reactions, electrochemical reactions at the surface of carbon steel, and the heterogeneous precipitation of iron carbonate (FeCO<sub>3</sub>) [1].

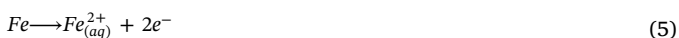
The water chemistry of dissolved CO<sub>2,(aq)</sub> involves the dissolution and hydration of CO<sub>2,(g)</sub> in water to form a weak carbonic acid:



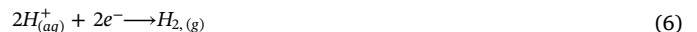
followed by two partial dissociation steps:



Iron is dissolved at the anodic sites to release ferrous ions:



Simultaneously, hydrogen ion reduction takes place at the cathodic site [2]:



FeCO<sub>3</sub> precipitates from solution when the concentration product of [Fe<sup>2+</sup>] and [CO<sub>3</sub><sup>2-</sup>] exceeds the solubility product, K<sub>sp</sub>, as defined by Eq. (7) [1], where [Fe<sup>2+</sup>]<sub>eq</sub> and [CO<sub>3</sub><sup>2-</sup>]<sub>eq</sub> are the equilibrium aqueous concentrations of Fe<sup>2+</sup> and CO<sub>3</sub><sup>2-</sup>.

$$K_{sp} = [Fe^{2+}]_{eq} [CO_3^{2-}]_{eq} \quad mol^2 \cdot L^{-2} \quad (7)$$

K<sub>sp</sub> is a function of temperature (T<sub>K</sub>) and ionic strength (I) [3]:

$$\log K_{sp} = -59.3498 - 0.041377T_K - \frac{2.1963}{T_K} + 24.5724 \log T_K + 2.518I^{0.5} - 0.657I \quad (8)$$

The ionic strength can be calculated from the concentration c<sub>i</sub> and charge z<sub>i</sub> of different species in the solution:

$$I = \frac{1}{2} \sum_i c_i z_i^2 \quad (9)$$

As one of the most common products of carbon steel corrosion in an aqueous CO<sub>2</sub> environment, FeCO<sub>3</sub> influences the corrosion process by precipitating on the steel surfaces [4,5]. A layer of FeCO<sub>3</sub> can form a

\* Corresponding author.

E-mail address: [zm735314@ohio.edu](mailto:zm735314@ohio.edu) (Z. Ma).

diffusion barrier for the corrosive species and, if well attached to the surface, significantly reduce the rate of electrochemical reactions and consequently the rate of general corrosion. Not every  $\text{FeCO}_3$  layer formed in reality is protective when the precipitation happens on an actively corroding steel surface. This is best characterized by the concept of scaling tendency [6]:

$$\text{Scaling Tendency} = \frac{\text{Precipitation Rate}}{\text{Corrosion Rate}} \quad (10)$$

suggesting that the protectiveness of  $\text{FeCO}_3$  layer is dependent on the competition between the precipitation and corrosion of the steel substrate surface. The  $\text{FeCO}_3$  layer is dense and protective only when the scaling tendency is higher than 1, i.e. when the amount of precipitation in the layer is much higher than the rate of steel corrosion underneath the layer. Otherwise, the formed  $\text{FeCO}_3$  layer will be porous and non-protective. Therefore, understanding the factors governing the rate of  $\text{FeCO}_3$  precipitation on a corroding surface is an important step in understanding the level of protectiveness it offers and the nature of the overall  $\text{CO}_2$  corrosion process.

Sun and Netic proposed a kinetic model (S&N Model, 2008) to calculate the  $\text{FeCO}_3$  precipitation rate [7]. The precipitation rate of  $\text{FeCO}_3$  is a function of the solubility saturation value of  $\text{FeCO}_3$  ( $S_{\text{FeCO}_3}$ ), and temperature, as shown by Eq. (11):

$$\text{PR} = k_r e^{-\frac{\Delta G}{RT}} K_{sp} (S_{\text{FeCO}_3} - 1) \quad \text{mol} \cdot \text{m}^{-2} \cdot \text{s}^{-1} \quad (11)$$

where

$k_r$ : kinetic constant,  $k_r = 1.8 \times 10^6 \text{ m}^4 \cdot \text{mol}^{-1} \cdot \text{s}^{-1}$

$\Delta G$ : activation energy of  $\text{FeCO}_3$  precipitation,  $\Delta G = 64,851.4 \text{ J} \cdot \text{mol}^{-1}$  and the saturation level of  $\text{FeCO}_3$ ,  $S_{\text{FeCO}_3}$ , is defined by

$$S_{\text{FeCO}_3} = \frac{[\text{Fe}^{2+}][\text{CO}_3^{2-}]}{K_{sp, \text{FeCO}_3}} \quad (12)$$

When comparing the S&N model with earlier models for  $\text{FeCO}_3$  precipitation rate calculation [6,8,9], it has been argued [7] that this model gives more realistic predictions, since it was based on the direct measurements of precipitated  $\text{FeCO}_3$  mass, rather than relying on the indirect measurement of  $\text{Fe}^{2+}$  concentration change in the bulk. Furthermore, it uses a more theoretically sound expression for the precipitation driving force: ( $S_{\text{FeCO}_3} - 1$ ), rather than the empirical expressions used by the other two models.

However, the experimental method used in development of the S&N's model was rather crude and time consuming, based on the measurements of time-averaged mass change of precipitated  $\text{FeCO}_3$ , taken before and after each exposure (typically lasting several hours). A more accurate technique that can provide real-time mass change monitoring throughout the experimental duration was thought to be essential for improving the accuracy of the S&N model. In addition, the S&N model was only validated at 80 °C; the model obviously needed to be validated over a broader temperature range to extend its validity for practical use.

In current work, a very accurate *in-situ* mass change measurement device – Electrochemical Quartz Crystal Microbalance (EQCM), was used as the primary experimental tool. EQCM relies on the piezoelectric properties of the quartz crystal substrate, as it oscillates at a specific frequency. A very small mass change on the quartz crystal surface will lead to a change in its oscillation frequency according to the simplified Sauerbrey equation [10]:

$$\Delta f = -C_f \cdot \Delta m \quad (13)$$

where

$\Delta f$ : frequency change, Hz

$C_f$ : the sensitivity factor for the quartz crystal, which is equal to  $56.60 \text{ Hz} \cdot \mu\text{g}^{-1} \cdot \text{cm}^2$  in current work

$\Delta m$ : the change in mass per unit area,  $\text{g} \cdot \text{cm}^{-2}$

It is important to mention that the Sauerbrey equation only applies to thin and rigid layers for which the energy dissipation during oscillations

can be ignored. To do so, the motional resistance has to be monitored, and only when it is constant – the changes in frequency can be linearly related to changes in mass. This is addressed further below in the section where procedure is explained.

Theoretically, this device can detect a mass change on the scale of nanograms. Besides the ability of monitoring the *in-situ* mass change in high resolution, the EQCM also allows to conduct electrochemical measurement simultaneously [11–13]. This makes the EQCM a good tool for the present study.

## 2. Experimental

### 2.1. Experimental methodology

This section presents the methodology developed for using the EQCM for the study of precipitation kinetics of  $\text{FeCO}_3$ . Different substrates were used for precipitation, in order to investigate how the nature of the substrate surface affects the kinetics of  $\text{FeCO}_3$  precipitation in an aqueous  $\text{CO}_2$  environment. Three sets of experiments were designed and conducted at different temperatures, and the results were compared with S&N model's calculations. Since the precipitation of  $\text{FeCO}_3$  is a relatively slow process, and is highly dependent on the saturation of  $\text{FeCO}_3$ , high initial saturation of  $\text{FeCO}_3$  were used for all experiments to speed up the process.

Experimental set #1:  $\text{FeCO}_3$  precipitation on a polarized gold (Au)-coated quartz crystal surface was conducted; gold was used due to being inert in this environment, and the precipitation of  $\text{FeCO}_3$  was the only process that affected the EQCM measurements. Polarization was done to simulate the corrosion potential seen with carbon steel corroding under similar conditions.

Experimental set #2:  $\text{FeCO}_3$  precipitation on a cathodically protected iron (Fe)-coated quartz crystal surface was conducted; this substrate is closer in nature to the carbon steel surface, yet the cathodic polarization was done to ensure that the substrate corrosion was minimized and the precipitation of  $\text{FeCO}_3$  was the dominant process affecting the EQCM measurements. It is understood that the local pH close to the substrate surface increased by applying cathodic polarization and could lead to an increase in the surface  $S_{\text{FeCO}_3}$ . However, the results show that this local condition had little effect of the  $\text{FeCO}_3$  precipitation kinetics, at least in the environments tested.

Experimental set#3:  $\text{FeCO}_3$  precipitation on an actively corroding iron (Fe)-coated quartz crystal surface was conducted; this is the most realistic situation, where both of the  $\text{FeCO}_3$  precipitation and spontaneous iron corrosion were occurring simultaneously at the substrate surface.

### 2.2. Apparatus

The EQCM device by Stanford Research System (QCM200) was used. The purchased 5 MHz At-cut Au-coated (about 0.5  $\mu\text{m}$  coating thickness) and Fe-coated quartz crystals (about 1  $\mu\text{m}$  coating thickness unless stated otherwise) with 1.37  $\text{cm}^2$  effective area are shown in Fig. 1. The coating metal is vapor deposited and bound to the silica



Fig. 1. Gold-coated and iron-coated quartz crystal.

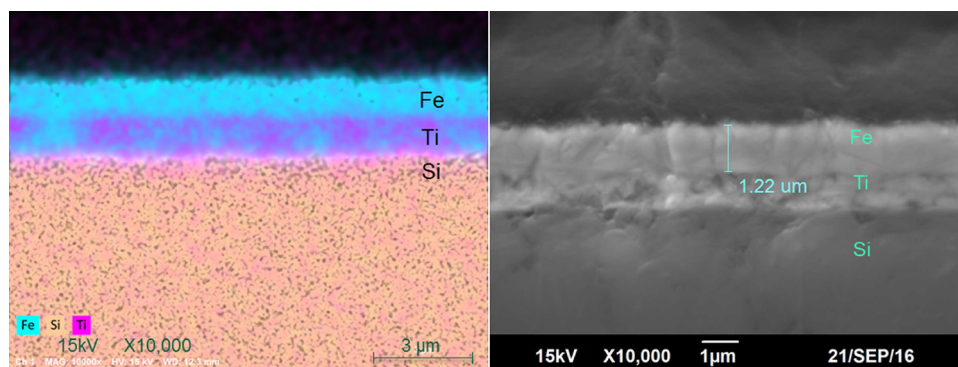


Fig. 2. Cross section images of an Fe-coated quartz crystal: EDS (left) and SEM (right).

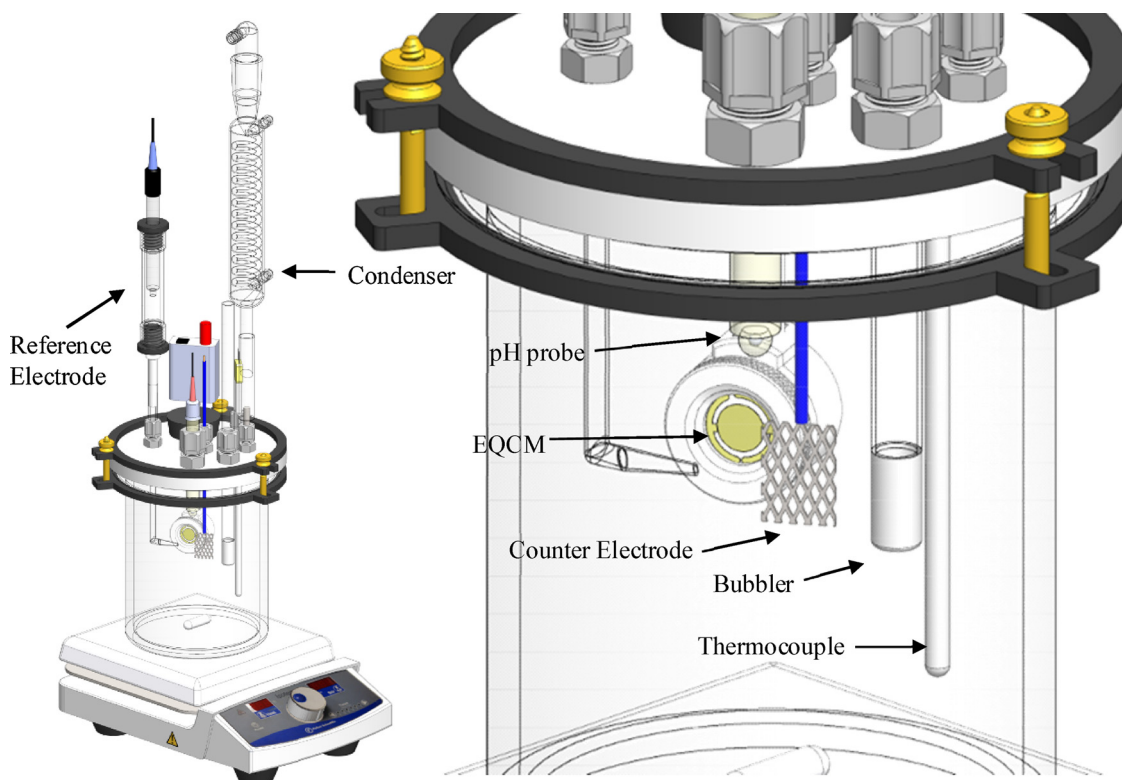


Fig. 3. Experimental set-up with EQCM (Image courtesy of Cody Shafer, ICMT).

substrate via a layer of adhesive materials as shown in Fig. 2 using Fe-coated quartz crystal as an example. The quartz crystal was then installed into the crystal holder, placed into a 2-liter glass cell (shown in Fig. 3) and served as the working electrode. The reference electrode was a saturated Ag/AgCl electrode and a platinum wire mesh was used as the counter electrode. A pH probe was immersed directly into the solution. A sparge tube was inserted into the solution to maintain a  $\text{CO}_2$  saturated condition throughout the experiment. The temperature of the solution was controlled by an immersed thermocouple connected to a heating plate.

### 2.3. Experimental procedure

The experimental matrix covering the three sets of experiments is shown in Table 1. All the experiments were conducted in a 1 wt.% NaCl solution. Before starting the experiment, the electrolyte was de-aerated by sparging with  $\text{CO}_2$  gas for at least 2 h and was maintained throughout the entire experiment. The solution temperature was set to

desired value, and the solution was adjusted to pH 6.60 by adding a deoxygenated  $\text{NaHCO}_3$  solution. Prior to immersion, the quartz crystal was cleaned with a  $\text{N}_2$  gas stream to remove any dust from the surface and installed into the EQCM holder. When needed, a specific potential was applied to the working electrode by using a potentiostat (Gamry Reference 600™). A deaerated ferrous chloride ( $\text{FeCl}_2 \cdot 4\text{H}_2\text{O}$ ) solution was added to provide dissolved  $\text{Fe}^{2+}$  and adjust the level of  $\text{FeCO}_3$  supersaturation. Samples of solution were drawn periodically from the glass cell with a syringe. Bulk pH were recorded and  $[\text{Fe}^{2+}]$  was measured by Genesys™ 10S Vis Spectrophotometer at the time each liquid sample was taken. At the meanwhile, the  $[\text{CO}_3^{2-}]$  was calculated based on solution pH, temperature, and the pressure of  $\text{CO}_2$  [1] to calculate the  $S_{\text{FeCO}_3}$  according to Eq. (13). Linear polarization resistance (LPR) was used to obtain corrosion rate measurements for the case when the iron coated quartz crystal was actively corroding. After the experiment, the surface of the quartz crystal specimen was analyzed by using scanning electron microscope (SEM).

**Table 1**  
Experimental matrix for FeCO<sub>3</sub> precipitation on different substrates.

| Description                           | Parameters                      |                                   |                                   |                    |
|---------------------------------------|---------------------------------|-----------------------------------|-----------------------------------|--------------------|
| Solution                              | 1 wt.% NaCl                     |                                   |                                   |                    |
| Total pressure/ bar                   | 1                               |                                   |                                   |                    |
| Purging gas                           | CO <sub>2</sub>                 |                                   |                                   |                    |
| Initial solution pH                   | 6.60 ± 0.05                     |                                   |                                   |                    |
| Stirring speed/ rpm                   | 50                              |                                   |                                   |                    |
| Materials                             | Etched Au-coated quartz crystal | Polished Fe-coated quartz crystal | Polished Fe-coated quartz crystal |                    |
| Polarization                          | −0.68 V vs. Sat. Ag/AgCl        | −0.05 ~ −0.1 V vs. OCP            | None (0 V vs. OCP)                |                    |
| Temperature/°C                        | 60, 70, 80                      | 50, 60, 70, 80                    | 50, 60, 70                        | 80                 |
| Initial S <sub>FeCO<sub>3</sub></sub> | ~600                            | ~600                              | ~600                              | 160, 300, 450, 600 |

#### 2.4. Calibration of the in-situ EQCM measurements

Before using the EQCM in the FeCO<sub>3</sub> precipitation study, it was important to prove that the EQCM was able to provide reasonable and accurate measurements under these conditions. So the first step was to calibrate the EQCM under CO<sub>2</sub> corrosion conditions. It was expected that the few microns thin iron layer on the quartz crystal will electrochemically dissolve (corrode) when it is exposed to the corrosive CO<sub>2</sub> environment and that this will result in a decrease of mass which is detectable by the EQCM. Calibration experiment was made by applying a fixed anodic current to the iron coated crystal (using the galvanostatic option of the potentiostat, and the Fe coating thickness used is about 0.5 μm), which should lead to a known and constant rate of iron dissolution. In an ideal case, assuming that the entire current was going towards the dissolution of iron, the mass loss and the anodic current can be correlated by using Faraday's law:

$$m = \frac{ItW}{nF} \quad (14)$$

Where,

*m*: mass change of metal, g

*I*: current, A

*t*: time, s

*W*: atomic weight of the metal, g • mol<sup>−1</sup>

*n*: valence charge of the dissolved metal in solution. *n* = 2 equivalents/mol for iron

*F*: faraday's constant. *F* = 96,485 C/equivalent

As shown in Fig. 4 (see highlighted part), a galvanostatic current of 8.6 A/m<sup>2</sup>, which is equivalent to a 10 mm/y corrosion rate was applied to the iron coated quartz crystal. As measured by the EQCM with *C<sub>f</sub>* = 56.60 Hz • μg<sup>−1</sup> • cm<sup>2</sup>, the mass change on the crystal surface was equivalent to

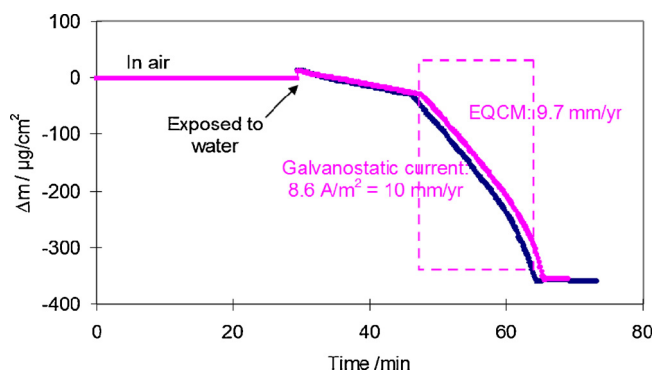


**Fig. 4.** Mass change of iron-coated quartz crystal when controlled by galvanostatic corrosion at 25 °C [14]. The two lines are from different experiments.

a 9.7 mm/y corrosion rate and the overall process showed good repeatability (3% error) [14]. A calibration followed the same procedure was also performed at 80 °C and the two methods agreed within 20% difference, by using the same value for *C<sub>f</sub>*. One possible reason for this was the known variation of *C<sub>f</sub>* with temperature. The sensitivity of measured frequency change to temperature, as reported by the instrument manufacturer is Δ*f* ≈ 8 Hz/°C, what amounts to Δ*f* ≈ 320 Hz over the 40 °C seen in the present study. When this is compared to the typical Δ*f* measured due to mass change caused by precipitation, which was of the order of 30,000 Hz, the error in assuming that the value for *C<sub>f</sub>* does not change with temperature is less than 1%. Therefore the higher level discrepancy between the galvanostatic and EQCM measurements is probably due to the inaccuracy of the assumptions underlying the electrochemical method.

#### 2.5. Procedure for FeCO<sub>3</sub> precipitation rate calculation

The methodology for calculating the precipitation rate of FeCO<sub>3</sub> from EQCM measurement is illustrated in Fig. 5. During the experiment, the pH value and [Fe<sup>2+</sup>] in the bulk solution were measured multiple times to get the saturation value of FeCO<sub>3</sub> according to Eq. (12). Due to the uncertainties associated with measurements of the bulk pH and [Fe<sup>2+</sup>], an estimate was made for the error in determining S<sub>FeCO<sub>3</sub></sub>. Given that the accuracy of measuring the pH was found to be approximately 0.1 pH unit and the accuracy of the [Fe<sup>2+</sup>] measurement was up to 1% of the measurement range, this translates into a 12% error in determining S<sub>FeCO<sub>3</sub></sub>. The corresponding error bars were added to all the graphs below. The error in measuring the mass change due to precipitation using the EQCM was so small that it cannot be shown adequately on the plots below (the error bars are much smaller than the symbols used).

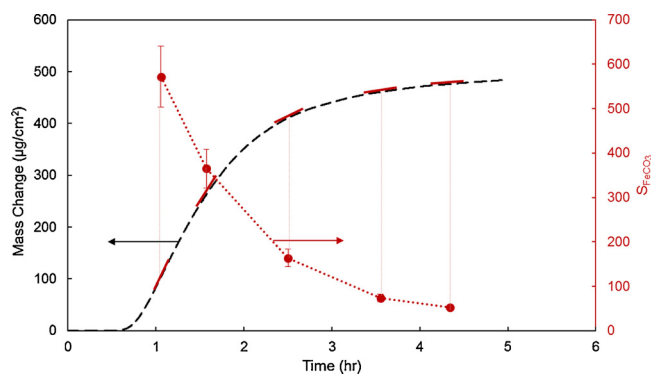


**Fig. 5.** Illustration of FeCO<sub>3</sub> precipitation rate calculation from in-situ mass change monitored by EQCM. Polarized Au-coated quartz crystal, pH 6.60, initial S<sub>FeCO<sub>3</sub></sub> = 600, 80 °C.

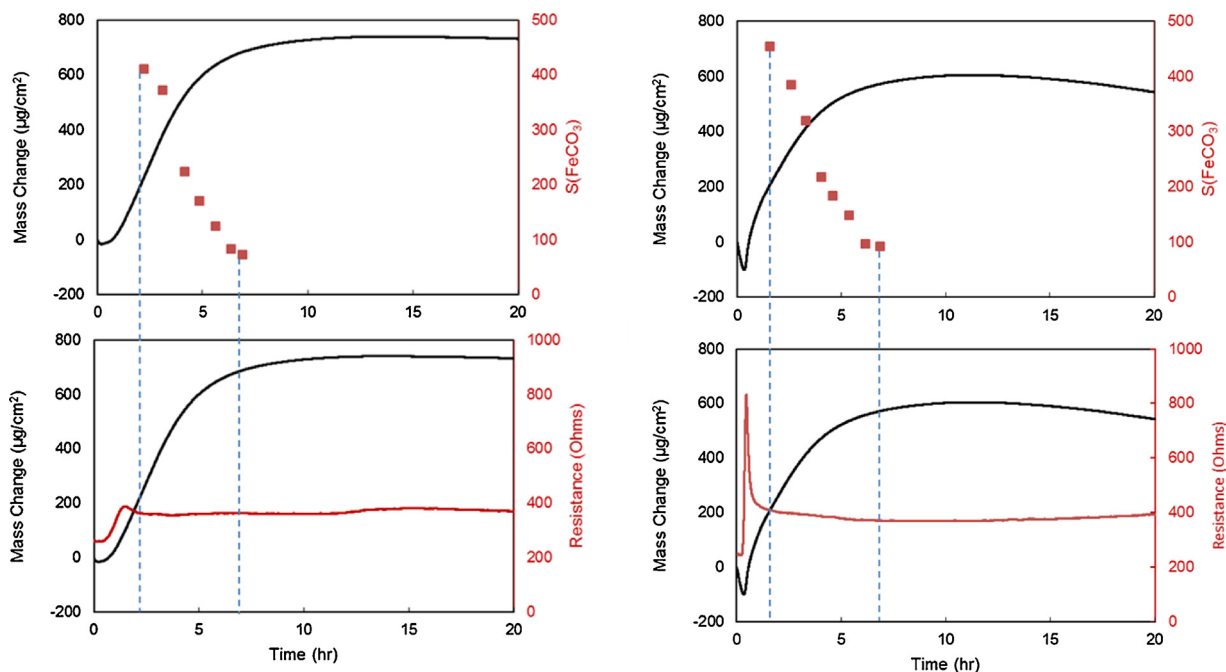


Fig. 6. Mass change,  $S_{\text{FeCO}_3}$ , and motional resistance obtained on a polarized Fe-coated crystal (left) and an actively corroding Fe-coated crystal (right) at 70 °C, pH 6.60.

Fig. 5 shows that the mass change monitored by EQCM increased due to the precipitation on the surface of the quartz crystal. Based on this information, the instantaneous slope was calculated (mass changes per unit area vs. time that is proportional to the precipitation rate) at the specific times when the pH value and  $[\text{Fe}^{2+}]$  were measured. The measured precipitation rates were converted from  $\mu\text{g} \cdot \text{cm}^{-2} \cdot \text{s}^{-1}$  to  $\text{mol} \cdot \text{m}^{-2} \cdot \text{s}^{-1}$  for easier comparison with the S&N model. Even though the  $\text{FeCO}_3$  precipitation is a two-step process that includes both the nucleation and growth steps, the current work focuses on the crystal growth step only. Nucleation step is often very short and surface dependent [15], while the crystal growth step is more universal and relevant for understanding of the formation of corrosion product layers.

The motional resistance of the quartz crystals was also monitored during this test (and every subsequent test), as significant fluctuations in this resistance could invalidate the use of the Sauerbrey equation. The motional resistance corresponds to the oscillation energy dissipation and it becomes more important when the EQCM is in direct contact with liquids and viscoelastic films. Fig. 6 presents the measurements of the motional resistance and how they relate to the mass change curve and saturation values of  $\text{FeCO}_3$ . The experiments were running at 70 °C using Fe-coated quartz crystals. The motional resistance changed significantly only during the initial stage of the experiment, which is the period in which the de-aerated ferrous chloride solution was just added to the solution to adjust the level of  $\text{FeCO}_3$  saturation. This led to changes in both the solution density and viscosity, as well as the surface morphology of the Fe-coated quartz crystal, since the  $\text{FeCO}_3$  started to nucleate on the substrate surface. However, the motional resistance was stable during the time window when the mass change rate measurements were taken, those that were used for precipitation rate calculation (the period between the two dashed lines in Fig. 6). This suggests that the  $\text{FeCO}_3$  layer forming within this time window was thin and rigid, and that the Sauerbrey equation held true.

### 3. Experimental results and discussion

#### 3.1. Validation of the $\text{FeCO}_3$ precipitation rate measurements using EQCM at 80 °C

The validation of the methodology for the precipitation rate measurements using the EQCM is presented in Fig. 7. Experimental results

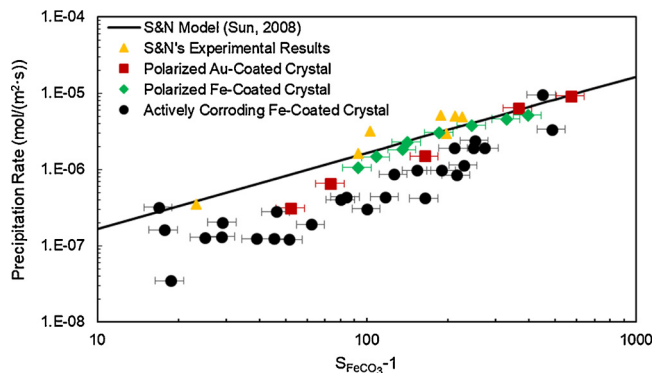


Fig. 7. Comparison among S&N model calculation, S&N precipitation rate results on carbon steel, and the precipitation rate results using the EQCM on polarized Au-coated quartz crystal, polarized Fe-coated quartz crystal, and actively corroding Fe-coated quartz crystal at 80 °C, pH 6.60.

on polarized Au-coated crystal, polarized Fe-coated crystal, and actively corroding Fe-coated crystal are included there, along with the original mass-change precipitation rate measurements of Sun and Nescic, used to develop the S&N model. For the precipitation on both polarized Au-coated quartz crystal and polarized Fe-coated quartz crystal, one set of measurements is shown with an initial  $S_{\text{FeCO}_3}$  around 600, while for the precipitation on actively corroding Fe-coated quartz crystal, the precipitation experiments were repeated four times using different initial  $S_{\text{FeCO}_3}$  as noted in Table 1.

The experimental results shown in Fig. 7 obtained on the actively corroding Fe-coated crystal exhibit reasonable consistency, with most of the results being within a factor of 3 of each other. This may sound like a significant degree of scatter, however, one needs to keep in mind that heterogeneous precipitation is notoriously difficult to reproduce, as small variations in the solution composition or substrate preparation may lead to significant changes in the kinetics of precipitation [16]. It can also be argued that the precipitation rates on polarized Au-coated crystal and polarized Fe-coated crystal were within the margin of scatter of the results obtained on the actively corroding Fe-coated crystal, i.e. they were similar in magnitude. Therefore both gold and

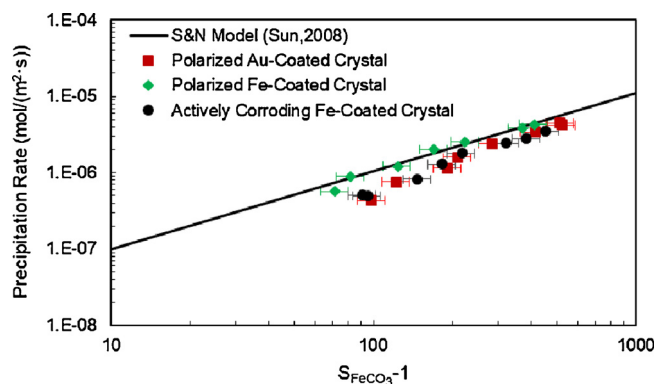


Fig. 8. Precipitation rates comparison between model calculation and the experimental results on different substrates at 70 °C, pH 6.60.

iron were used as substrates in subsequent experiments. When the present experimental precipitation rates obtained from the EQCM are compared with the experimental S&N results obtained by the mass-change method, a similar exponent with respect to  $S_{\text{FeCO}_3}$  of approximately 1 is obtained (1.4 for Au-coated crystal, 1.1 for both polarized Fe-coated crystal and actively corroding Fe-coated crystal, and 1.2 for S&N experimental results conducted on an actively corroding steel surface). This implies a linear relationship between precipitation rate and  $S_{\text{FeCO}_3}$ . Other authors have proposed different values for the exponent (i.e.  $\text{PR} \propto (S_{\text{FeCO}_3}^{0.5}-1)^2$  from both Greenberg and Tomson [8], and Johnson and Tomson [9];  $\text{PR} \propto (S_{\text{FeCO}_3}-1)(1-S_{\text{FeCO}_3}^{-1})$  from Van Hunnik et al. [6]) which are not supported by this work. Overall, the S&N results are higher approximately by a factor of 5, what is not surprising, given that the data are obtained through two very different techniques, that the experiments were conducted on different substrates and that S&N reported time-averaged precipitation rates (over 2–3 hour exposures), while the present results are reflecting instantaneous precipitation rate measurements. The S&N model is also shown, being somewhere in between the S&N and the present measurements. Overall, it can be concluded that the EQCM technique was validated for the precipitation rate measurements, presented below.

### 3.2. Precipitation rates of $\text{FeCO}_3$ at 70 °C

The experimental  $\text{FeCO}_3$  precipitation rates on different substrates are presented in Fig. 8 for 70 °C. At this temperature, all the results are closer together when compared to 80 °C. The precipitation rates measured on polarized Au-coated crystal overlap with the results obtained on the actively corroding Fe-coated crystal. However, the precipitation rates measured on Au are certainly affected by the very different nature of the substrate. It is believed that the precipitation kinetics are lower due to differences in the nucleation process. For the case of actively corroding Fe-coated crystal, both  $\text{FeCO}_3$  precipitation and spontaneous iron substrate dissolution occur simultaneously. Therefore, the total mass change captured by the EQCM is equal to the precipitation mass gain minus the corrosion mass loss. Furthermore, the rate of  $\text{FeCO}_3$  precipitation on a corroding iron surface is affected by the “disappearing” substrate surface (making it harder to nucleate). At the same time, this corrosion leads to the generation of extra  $\text{Fe}^{2+}$  ions at the substrate surface, thereby increasing the level of surface supersaturation what makes nucleation and crystal growth faster. It is difficult to resolve which of these effects dominate. Therefore, neither Au nor the actively corroding Fe surface present an ideal substrate for measuring the  $\text{FeCO}_3$  precipitation kinetics.

To compensate for the mass change error introduced by the corrosion of Fe, the corrosion mass loss was calculated from LPR results and this mass was then added to the EQCM measured mass gain for the Fe-coated crystal. The precipitation rates before and after this

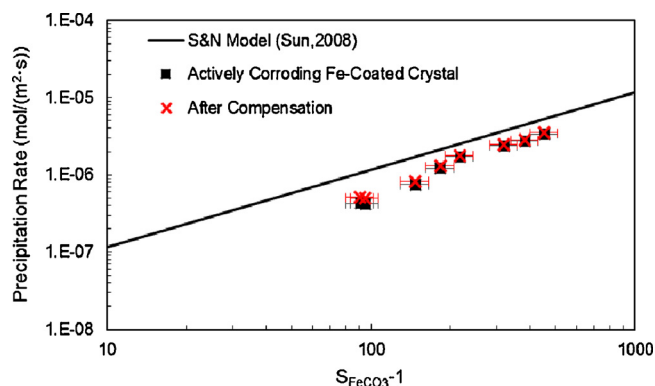


Fig. 9. Comparison for the experimental results with and without mass compensation, and model calculation for 70 °C, pH 6.60.

compensation are compared in Fig. 9. The overall change is relatively small. At lower  $S_{\text{FeCO}_3}$  values, the total mass change is affected more by the compensation, because of the low precipitation rates. Similar phenomenon has been reported by S&N who used an actively corroding carbon steel as the substrate [7].

Applying cathodic polarization to the Fe-coated crystal minimizes the effect of active iron substrate dissolution, making it the most suitable method for measuring the kinetics of  $\text{FeCO}_3$  precipitation. The measurements taken on the polarized Fe-coated crystal are also shown in Fig. 8 and on average they are higher than those obtained on polarized Au-coated crystal (up to 50%) and compensated actively corroding Fe-coated crystal (up to 40%).

Finally, the S&N model calculation are also shown in Fig. 8 as a line, agreeing exceptionally well with the results obtained on polarized Fe-coated crystal (within 8%). At the same time, the precipitation rates calculated from the S&N model are up to 60% higher than the experimental results obtained on the surface of polarized Au-coated crystal and the actively corroding Fe-coated crystal.

### 3.3. Precipitation rates of $\text{FeCO}_3$ at 60 °C

The experimental  $\text{FeCO}_3$  precipitation rates on different substrates are presented in Fig. 10 for 60 °C. The data shown for each of the Fe-coated crystals come from two independent experiments (four in total), yet their overlap is within the margin of scatter. The precipitation rates measured on polarized Au-coated crystal at 60 °C are 2–3 times lower than those measured on the actively corroding Fe-coated crystal and almost an order of magnitude lower than what is obtained on a polarized Fe-coated crystal, what is quite different from results obtained at 80 °C and 70 °C. This supports the fact that the precipitation kinetics on

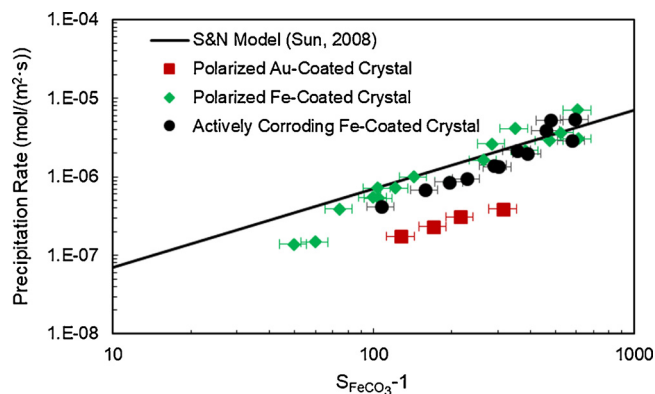


Fig. 10. Precipitation rates comparison between model calculation and experimental results using the EQCM on different substrates at 60 °C, pH 6.60.

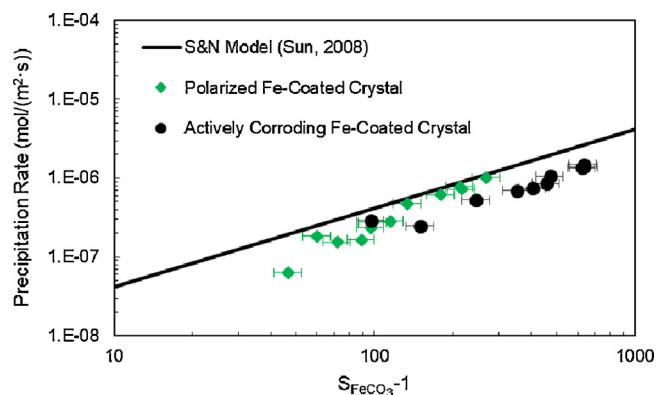


Fig. 11. Precipitation rates comparison between model calculation and experimental results using the EQCM on different substrates at 50 °C, pH 6.60.

Au is affected by a lower nucleation rate of  $\text{FeCO}_3$ , when compared to that obtained on Fe. The differences in nucleation rates on different substrates are less pronounced at higher temperatures when the overall precipitation kinetics is fast. At a sufficiently low temperature, the slow nucleation on Au becomes the rate determine step and retards the kinetics of the entire precipitation process. Therefore, the precipitation rate of  $\text{FeCO}_3$  measured on polarized Au-coated crystal is considered to be an inaccurate representation of what happens on a steel surface at this temperature.

When comparing the  $\text{FeCO}_3$  precipitation on the two Fe-coated crystals, the precipitation rates on polarized Fe-coated crystal are slightly higher than those obtained on actively corroding Fe-coated crystal (approximately up to a factor of 2). The S&N model calculation are also shown in Fig. 10 as a line, agreeing best with the measurements obtained on polarized Fe-coated crystal (most of data points are within a factor of 2).

#### 3.4. Precipitation rates of $\text{FeCO}_3$ at 50 °C

The experimental  $\text{FeCO}_3$  precipitation rates on Fe-coated crystal are presented in Fig. 11 for 50 °C. Au-coated crystal results are not shown because at this temperature it was impossible to conduct valid and repeatable experiments, due to the very low and erratic rate of nucleation of  $\text{FeCO}_3$  on Au. The results shown for the two Fe-coated crystals come from two independent series of experiments and overlap within the margin of experimental error.

Similarly to what has been seen at the higher temperatures, the precipitation rates of  $\text{FeCO}_3$  obtained on polarized Fe-coated crystal are higher than those seen on the actively corroding Fe-coated crystal, by a similar margin and for the same reasons. The S&N model calculation are also shown in Fig. 11, being fairly close to most of the data points obtained on polarized Fe-coated crystal.

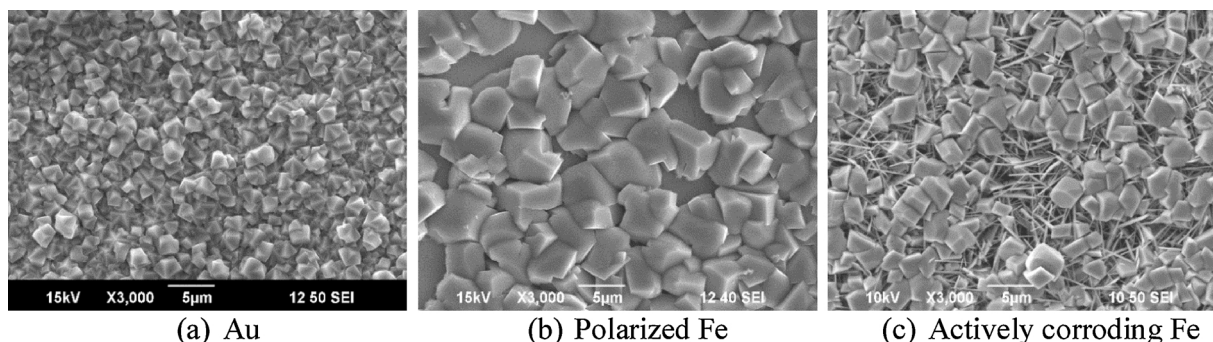


Fig. 12. SEM analysis of precipitated  $\text{FeCO}_3$  on (a) Au-coated crystal, (b) Polarized Fe-coated crystal, and (c) Actively corroding Fe-coated crystal at 70 °C, pH 6.60.

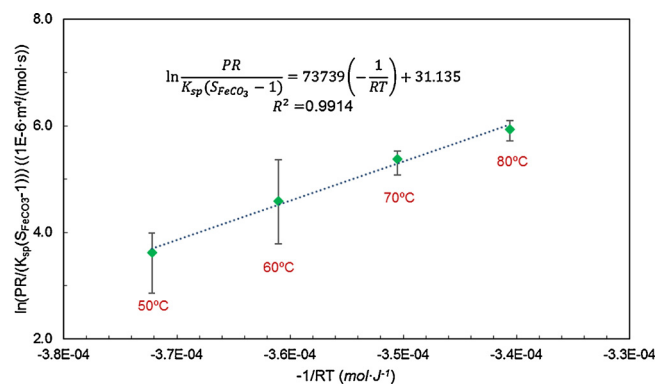


Fig. 13. The best fit line for activation energy and kinetic constant in the  $\text{FeCO}_3$  precipitation rate equation.

#### 3.5. Precipitation rates of $\text{FeCO}_3$ at 40 °C

$\text{FeCO}_3$  could still be precipitated on polarized Fe-coated crystal at 40 °C, the repeatability of the experiments was poor. It is believed that the  $\text{FeCO}_3$  nucleation rate on polarized Fe-coated crystal is so slow at this temperature that the overall precipitation process becomes erratic and irreproducible. When using the actively corroding Fe-coated crystal, no mass gain was detected by EQCM, indicating that the mass decrease due to the substrate dissolution is higher than the mass increase due to the  $\text{FeCO}_3$  precipitation. The thin coating of Fe on the quartz crystal was dissolved completely by the end of the experiment, suggesting that the slow precipitation of  $\text{FeCO}_3$  at this temperature was overpowered by the faster corrosion rate of Fe (dissolution of the substrate). Due to the fact that no measurable precipitation was obtained on Au already at 50 °C, this substrate was not used at 40 °C.

#### 3.6. Surface analysis of the precipitated $\text{FeCO}_3$

As an example of the morphologies obtained in different experiments, Fig. 12 presents a sample of the many SEM surface images of the precipitated  $\text{FeCO}_3$  on the Au-coated crystal, polarized Fe-coated crystal, and actively corroding Fe-coated crystal at 70 °C. From these images, it may appear that quite different  $\text{FeCO}_3$  morphologies have formed on different substrates, e.g. there are only prism-shaped  $\text{FeCO}_3$  crystals on Au, similar but larger crystals on polarized Fe and both prism-shaped and plate-shaped  $\text{FeCO}_3$  crystals on actively corroding Fe. However, these types of variations have been seen on the same samples at different locations of the surface and likewise there was quite a bit of variation on the same substrate from one repeat to another. Yet, the precipitation rate data seem to be relatively coherent, as shown above. The cause of this variation is not fully understood at this point but should bear little influence on the precipitation kinetics, what is the primary purpose of the present study.

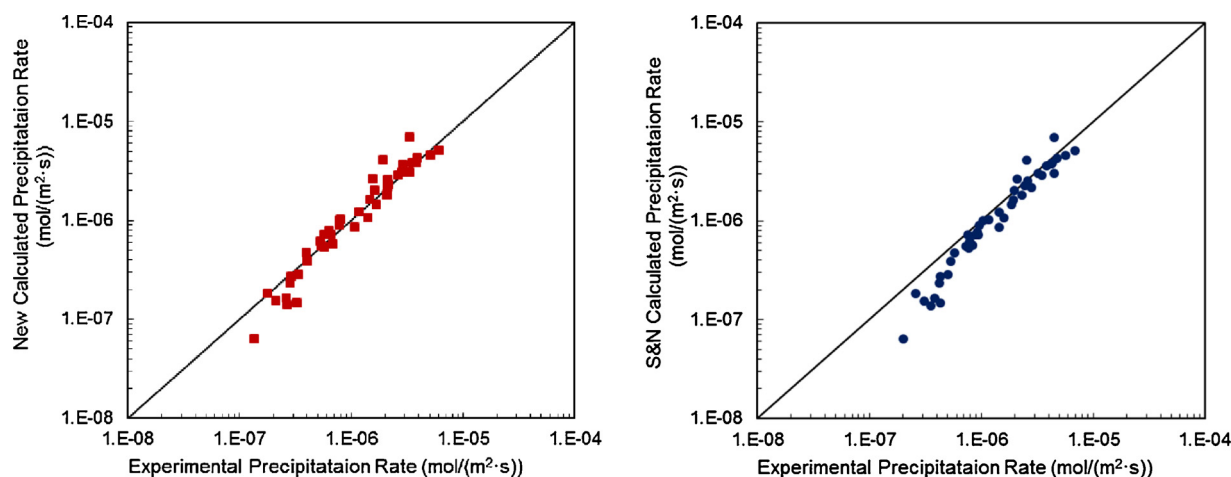


Fig. 14. Parity plot comparison of experimental precipitation rate and the calculated precipitation rate using current improved constants (left) and S&N model (right).

#### 4. Activation energy and kinetic constant in the $\text{FeCO}_3$ precipitation rate equation

The previous section shows a rather good agreement, between the experimental  $\text{FeCO}_3$  precipitation rate results obtained by EQCM in the present study, and by the S&N's  $\text{FeCO}_3$  equation. Nevertheless, new values for the activation energy and kinetic constant were extracted from the experimental data and compared to those initially developed for in the S&N's equation.

By taking a natural logarithm of both sides of Eqs. (11) and (15) can be obtained:

$$\ln \frac{PR}{K_{sp} \cdot (S_{\text{FeCO}_3} - 1)} = -\frac{\Delta G}{RT} + \ln k_r \quad (15)$$

Therefore, if  $\ln \frac{PR}{K_{sp} \cdot (S_{\text{FeCO}_3} - 1)}$  vs.  $(-\frac{1}{RT})$  is plotted, a straight line should theoretically be obtained with the slope being equal to the activation energy  $\Delta G$  and the y intercept being the  $\ln k_r$ , as shown in Fig. 13. The best fit line yielded  $\Delta G = 73,739 \text{ J} \cdot \text{mol}^{-1}$  and  $k_r = 3.32 \times 10^7 \text{ m}^4 \cdot \text{mol}^{-1} \cdot \text{s}^{-1}$  by using the average experimental value at each temperature. As a comparison, the S&N's  $\text{FeCO}_3$  precipitation rate equation uses  $\Delta G = 64,851.4 \text{ J} \cdot \text{mol}^{-1}$  and  $k_r = 1.8 \times 10^6 \text{ m}^4 \cdot \text{mol}^{-1} \cdot \text{s}^{-1}$ .

The parity plots that compares the experimental  $\text{FeCO}_3$  precipitation rate data with the calculated  $\text{FeCO}_3$  precipitation rate data are shown in Fig. 14 for the current model with the new constants (left) and S&N model (right). In an ideal case, all the points should fall onto the diagonal. One can see that for both models, the agreement is rather good, yet the points on the left plot distribute more evenly around the diagonal line, indicating a better fit. The improvement seems to be most significant at the lower precipitation rates obtained for the smallest saturation values.

#### 5. Conclusions

- Three different substrates were used to conduct the  $\text{FeCO}_3$  precipitation experiments:
  - a cathodically polarized gold-coated quartz crystal,
  - a freely corroding iron-coated quartz crystal and
  - a cathodically polarized iron-coated quartz crystal,
- By using EQCM, repeatable and consistent precipitation rates were obtained across different substrates, in the temperature range 50–80 °C. Experiments conducted on a cathodically polarized iron-coated crystal tend to minimize the influence of surface dissolution.
- The obtained precipitation rates were used to determine the theoretical kinetic constant and the activation energy for the

precipitation rate equation, which were then compared with those reported in the Sun and Nescic model (2008). An overall improvement was obtained particularly at the lower saturation levels.

#### Acknowledgments

The authors would like to express sincere appreciation to the following industrial sponsors for their financial support and direction: Anadarko, Baker Hughes, BP, Chevron, CNOOC, ConocoPhillips, DNV GL, ExxonMobil, M-I SWACO, Occidental Oil Company, Petroleum Institute, PTT, Saudi Aramco, Shell Global Solutions, Sinopec, TransCanada, TOTAL, and Wood Group Kenney.

#### References

- [1] S. Nešić, W. Sun, Corrosion in acid gas solutions, in: B. Cottis, M. Graham, R. Lindsay, S. Lyon, T. Richardson, D. Scantlebury, H. Scott (Eds.), *Shreir's Corrosion*, Elsevier, Amsterdam, 2010, pp. 1270–1298.
- [2] T. Tran, B. Brown, S. Nešić, Corrosion of Mild Steel in an Aqueous  $\text{CO}_2$  Environment – Basic Electrochemical Mechanisms Revisited, *CORROSION/2015*, Dallas, TX, 2015.
- [3] W. Sun, S. Nešić, R.C. Woollam, The effect of temperature and ionic strength on iron carbonate ( $\text{FeCO}_3$ ) solubility limit, *Corros. Sci.* 51 (2009) 1273–1276.
- [4] J.E. Oddo, M.B. Tomson, The Prediction of Scale and  $\text{CO}_2$  Corrosion in Oil Field Systems, *CORROSION/1999*, San Antonio, TX, 1999 paper no. 41.
- [5] A.K. Dunlop, H.L. Hassell, P.R. Rhodes, Fundamental Considerations in Sweet Gas Well Corrosion, *CORROSION/1983*, Anaheim, CA, 1983 paper no. 46.
- [6] E. Van Hunnik, B.F.M. Pots, E.L.J.A. Hendriksen, The Formation of Protective  $\text{FeCO}_3$  Corrosion Product Layers in  $\text{CO}_2$  Corrosion, *CORROSION/1996*, Houston, TX, 1996 paper no. 6.
- [7] W. Sun, S. Nešić, Kinetics of corrosion layer formation: part 1—Iron carbonate layers in carbon dioxide corrosion, *Corros. J.* 64 (2008) 334–346.
- [8] J. Greenberg, M. Tomson, Precipitation and dissolution kinetics and equilibria of aqueous ferrous carbonate vs. Temperature, *Appl. Geochem.* 7 (1992) 185–190.
- [9] M.L. Johnson, M.B. Tomson, Ferrous Carbonate Precipitation Kinetics and Its Impact on  $\text{CO}_2$  Corrosion, *CORROSION/1991*, Houston, TX, 1991 paper no. 268.
- [10] G. Sauerbrey, Verwendung von schwingquarzen zur wägung dünner schichten und zur mikrowägung, *Zeitschrift für physik* 155 (1959) 206–222.
- [11] R. Oltra, I.O. Efimov, Calibration of an electrochemical quartz crystal microbalance during localized corrosion, *J. Electrochem. Soc.* 141 (1994) 1838–1842.
- [12] C. Gabrielli, M. Keddam, A. Khalil, G. Maurin, H. Perrot, R. Rosset, M. Zidoune, Quartz crystal microbalance investigation of electrochemical calcium carbonate scaling, *J. Electrochem. Soc.* 145 (1998) 2386–2396.
- [13] C. Gabrielli, S. Joiret, M. Keddam, H. Perrot, N. Portail, P. Rousseau, V. Vivier, A SECM assisted EQCM study of iron pitting, *Electrochim. Acta* 52 (2007) 7706–7714.
- [14] Y. Yang, B. Brown, S. Nešić, Application of EQCM to the study of  $\text{CO}_2$  corrosion, 17th International Corrosion Congress, Las Vegas, NV, 2008.
- [15] X.Y. Liu, Generic Mechanism of heterogeneous nucleation and molecular interfacial effects, in: Y. Furukawa, K. Nakajima (Eds.), *Advances in Crystal Growth Research*, Elsevier Science B.V., Amsterdam, 2001, pp. 42–61.
- [16] F.L. Binsbergen, Heterogeneous nucleation of crystallization, *Prog. Solid State Chem.* 8 (1973) 189–238.